ELSEVIER

Carbohydrate Research 263 (1994) 197–207

CARBOHYDRATE RESEARCH

The thermodynamic characteristics of the conformational transitions of native xanthan

Leon Bezemer, Maxim E. Kuil, Jaap C. Leyte *

Department of Physical and Macromolecular Chemistry, Gorlaeus Laboratories, Leiden University, P.O. Box 9502, 2300 RA Leiden, Netherlands

Received 25 February 1994; accepted 16 May 1994

Abstract

Xanthan shows a well-known conformational transition in salt free solution at slightly elevated temperature, upon charging. Recently, a second transition was reported at higher temperature, when potentiometric results were analyzed using a Henderson–Hasselbalch representation of the titration curves. The molar fractions of the xanthan monomers in the different conformational states **A**, **B**, and **C** could then be determined as a function of the degree of proton dissociation, θ. Here it is shown that a simple linear dependence of the standard free enthalpy changes (ΔG^0) of the transitions on θ adequately describes the changing molar fractions throughout the titration curves. From a temperature series of the first transition (**A** → **B**), the dependence of the changes of standard enthalpy and entropy on θ, $\Delta H^0(\theta)$, and $\Delta S^0(\theta)$ are inferred. Surprisingly, irrespective of the degree of dissociation, the **A** → **B** transition is dominated by the change of standard entropy of the transition. Beyond $\theta \approx 0.3$ the **B** state is entropy stabilized relative to the **A** state. The dependence of the thermally induced transitions on the polymer charge is illustrated with viscosity data.

Keywords: Xanthan; *Xanthomonas campestris*; Conformational transitions

1. Introduction

Native xanthan is an extracellular microbial polysaccharide, produced by fermentation of *Xanthomonas campestris* [1]. The molecular weight is of the order 10^7 Da, with a relatively large polydispersity ($M_w/M_n \approx 2$–3) [2–4]. The repeat unit consists of a cellulose backbone, bearing a trisaccharide side-chain, which can be charged by titration on every second glucosyl residue [5,6]. For the secondary structure there is no generally accepted model; xanthan is thought to be made up of either double helices [7,8] or to exist as side-by-side aggregated single helices [9].

* Corresponding author.

SSDI 0008-6215(94)00171-B

A conformational transition, observable as a sigmoidal change of many physico-chemical properties, e.g., viscosity, optical rotation, and circular dichroism, is known to take place at elevated temperatures [1,10,11] or if the highly charged polymer is poorly screened. A clear demonstration of the effects of polymer charge on the conformational transition, is an optical rotation study with samples of different degree of dissociation (ionization) in Ref [12]. The screening effect of added salt on the transition is demonstrated in optical rotation studies reported in Refs [10 and 11] and [12]. The nature of this transition and the ordered and disordered states before and after the transition are still a matter of debate. However, the observation of molecular weight invariance [8] and first-order kinetics [9] rule out the possibility of complete dissociation of double helices into single strands. It has been suggested that, in the ordered state, the side chains may be folded around the backbone [13], and since the majority of the polymer mass is situated in the side chain, a possible mechanism for the transition is the unfolding of the side chains from the backbone. Recently, NMR measurements [14] indicated an enhanced mobility of the side chains in the premelting region which supports this reasoning.

In a recent study [15] of the potentiometric titrations and the rotational viscosity of isotropic, aqueous solutions of biochemically purified, native xanthan ($C_p = 2$ mM) at several temperatures and ionic strengths we did not only observe the well known sigmoid conformational transition ($\mathbf{A} \rightarrow \mathbf{B}$), but we also observed the occurrence of a second transition ($\mathbf{B} \rightarrow \mathbf{C}$), presumably of conformational origin, not reported before. The variation in the titration curves, i.e., pK_a versus θ, strongly depends on the temperature and concentration of added salt. Increasing either temperature or salt concentration leads in general to an increase of pK_a. The glass-calomel electrode gradually contaminates the solution with KCl up to a concentration of 0.5 mM, and a gradual but very small increase of the pK_a (< 0.1 units) is expected over the entire titration curve. With more than 5 mM of added salt, the contamination can be neglected and at higher temperature a downward curvature in the titration curves is observed. Using a Henderson–Hasselbalch representation, this curvature can be related to the $\mathbf{A} \rightarrow \mathbf{B}$ transition.

Without added salt, despite the expected contamination effect, a downward curvature is also observed. For $T \leq 43$°C, the Henderson–Hasselbalch representation can be analyzed with a two state model ($\mathbf{A} \rightarrow \mathbf{B}$), but for $T > 43$°C a three state model ($\mathbf{A} \rightarrow \mathbf{B} \rightarrow \mathbf{C}$) is required. At 63°C, the first and second transition can be suppressed by addition of 39 and 5 mM NaCl, respectively. The conformational transitions are not suppressed by the introduction of the Na^+ counterion, to a final concentration of 2 mM, upon neutralisation.

We were able to detect this second transition since we extended the experimental range of investigation to salt concentrations as low as 0.5 mM at temperatures as high as 63°C. Most of the previous work in the literature deals with higher ionic strengths.

In the literature, the thermodynamic analysis of the conformational transition of xanthan has been restricted to the determination of the standard enthalpy in DSC experiments [9,16] and to the determination of the activation enthalpy and entropy [9]. In this article, we deduce from the titration results, the standard free enthalpy (ΔG^0) of both transitions, and from a temperature series also the standard enthalpy (ΔH^0) and standard entropy (ΔS^0) of the $\mathbf{A} \rightarrow \mathbf{B}$ transition as a function of the degree of proton dissociation θ. To this end the experimentally observed linear dependence of $\ln K = -\Delta G^0/RT$ on the degree of dissociation θ is taken to be valid in the whole transition region, i.e., outside the limited region

where it could be established with sufficient experimental accuracy. The thermodynamic data show that increasing the temperature does not necessarily destabilize the "ordered" xanthan conformation. In fact, for the uncharged macromolecule the ordered conformation is relatively more stable at higher temperature. For $\theta > 0.3$ the transition may be induced thermally as demonstrated also by the viscosity results. For the experimental details of the titrations and the viscosity experiments the reader is referred to Ref [15].

2. Analysis of the conformational transitions

The **A** → **B** *transition.*—Consider the conformational equilibrium: **A** ⇄ **B**. The following expressions for the equilibrium constant K hold:

$$K = \frac{[\mathbf{B}]}{[\mathbf{A}]} \qquad K = \exp\left(\frac{-\Delta G^0}{RT}\right) \tag{1a,b}$$

For every θ there is thermodynamic equilibrium, but if θ is increased, the equilibrium shifts to the right hand side. Thus, K and consequently also ΔG^0, i.e., $G^0_B - G^0_A$, are not constant; they depend in fact on θ, the temperature, and the ionic strength. At constant temperature and ionic strength, K and ΔG^0 are functions of θ only. The following simple empirical relation was obtained from potentiometric titration results [15]:

$$K(\theta) = \exp\left(C_1 \cdot \theta - C_2\right) \tag{2}$$

C_1 and C_2 were found to be positive [15] which implies that the change of the standard free enthalpy of the transition **A** → **B** is decreased by adding charge to a monomer of the macromolecule in state **A**. The molar fraction of **B**, f_B, is given by the equations:

$$f_b = \frac{K}{1+K} \qquad f_b = \frac{\exp(C_1 \cdot \theta - C_2)}{1+\exp(C_1 \cdot \theta - C_2)} \tag{3a,b}$$

C_1 and C_2 have been estimated earlier [15] from the linear regression of ln K, but the regression is hampered by the correlation of the errors in the molar fractions of **A** and **B** which determine K. With Eqn. (3b), both C_1 and C_2 can be obtained from a direct fit of the composition curve, with the additional advantage that a larger data range can be used than with the previous method. Eqn. (3b) predicts a sigmoid-shaped transition with a peak-shaped first derivative curve with respect to θ, which is in agreement with the experimental results; this is demonstrated in Figs. 1 and 2. The midpoint of the transition, expressed as θ_m in these isothermal experiments, is found at the maximum.

The **B** → **C** *transition: the modified consecutive reaction.*—Consider the conformational equilibria: **A** ⇄ **B** ⇄ **C**. By analogy with Eqn. (1a):

$$K_1 = \frac{[\mathbf{B}]}{[\mathbf{A}]} \qquad K_2 = \frac{[\mathbf{C}]}{[\mathbf{B}]} \qquad K_1 K_2 = \frac{[\mathbf{C}]}{[\mathbf{A}]} \tag{4a,b,c}$$

$$K_1(\theta) = \exp(C_1 \cdot \theta - C_2) \qquad K_2(\theta) = \exp(C_3 \cdot \theta - C_4) \tag{5a,b}$$

The four parameters, C_1–C_4, can be obtained by fitting the composition curves, e.g., the molar fraction of component **C**, f_C, obtained as a function of θ from the Henderson–Hasselbalch analysis. During the **B** → **C** transition, the development of the molar fraction f_C of the final state **C**, is given by:

$$f_C = \frac{K_1 K_2}{1 + K_1 + K_1 K_2} = \frac{\exp[\,(C_1 + C_3)\cdot\theta - (C_2 + C_4)\,]}{1 + \exp(C_1\cdot\theta - C_2) + \exp[\,(C_1 + C_3)\cdot\theta - (C_2 + C_4)\,]} \qquad (6^{a,b})$$

The midpoints of the transitions.—The midpoints of the transitions, θ_{mI} and θ_{mII} can be obtained either by taking the derivative of the experimental composition curve with respect to θ, or from Eqn. (7) which follows from Eqns. (2) and (5).

$$\theta_{mI} = \frac{C_2}{C_1} \qquad \theta_{mII} = \frac{C_4}{C_3} \qquad (7^{a,b})$$

A comparison of the midpoints of transition in the empirical derivative curve with the theoretical values can serve as an additional check on the fitted constants.

3. Results

In Figs. 1a and b the results are shown of the fit of the composition curve and the residue at 43°C for Cs = 0.5 mM, a representative of the **A** → **B** type transition [15]. The fits of the other **A** → **B** cases at 25°C for Cs = 0.5 mM and 63°C for Cs = 5 mM are of similar quality and hence not shown. The error bars in the composition curve were calculated with standard error analysis, taking the derivatives of the expression for f_B, Eqn. (7b) of Ref [15], with respect to the degrees of dissociation θ (of the solution), α (of the **A** state) and β (of the **B** state) combined with an assumed standard deviation of 0.5% for the degrees of dissociation θ, α, and β. The drawn lines are the theoretical fits of the data to Eqn. (3b). The residues of the fit are very small for all three **A** → **B** cases.

A disadvantage of the Henderson–Hasselbalch analysis of the titrations is that a complete transition is assumed and the original composition curves of Ref [15] run from 0 to 1. However, as we have suggested before [15], at 25°C and $\theta = 1$ only the first part and not the entire *s*-shaped curve is observed, which is an indication that the first transition is not complete at 25°C. The experimental maximum of the derivative of the *s*-shaped composition curves is now used to check the midpoint of the transition and to rescale the composition curve at 25°C accordingly. Fig. 2 shows a maximum at the θ value for which $f_B = 0.86$. By definition, however, this maximum must correspond with the midpoint at which $f_B = 0.5$. The entire composition curve is thus rescaled by multiplication with the factor 0.5/0.86. This rescaled composition curve of 25°C/Cs = 0.5 mM and the original composition curves of 43°C/Cs = 0.5 mM and 63°C/Cs = 5 mM were fitted with a least squares method to the function of Eqn. (3b). After rescaling, the results of 25°C are in better agreement with the results of the other two **A** → **B** cases. First, the apparent linear branch of the **B** state in the Henderson–Hasselbalch representation of 25°C was recalculated with Eqns. (7a,b), (5b), and (3) of Ref [15] after rescaling, and the new slope ($n_B = 1.25$) and intercept ($pK_0^B = 3.32$) show more consistency with the slopes and intercepts of the other two **A** → **B**

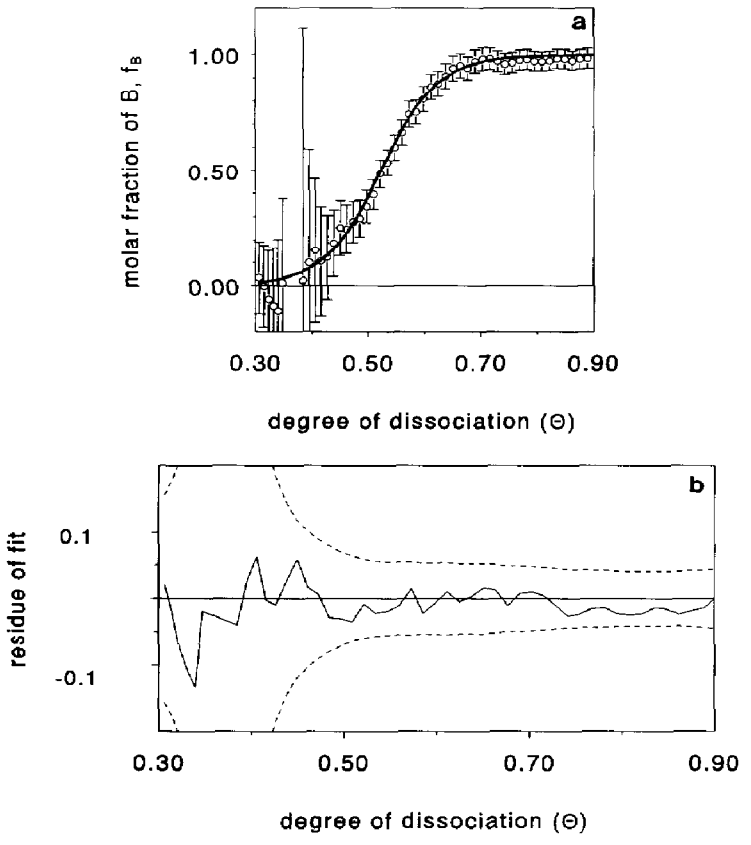

Fig. 1. (a) Composition curve at 43°C and Cs = 0.5 mM, f_B versus θ (**A** → **B** case). The drawn line is the fit using Eqn. 3b. (b) Residue plot of the fit. The dotted lines represent one standard deviation, the drawn line is the difference between fit and curve.

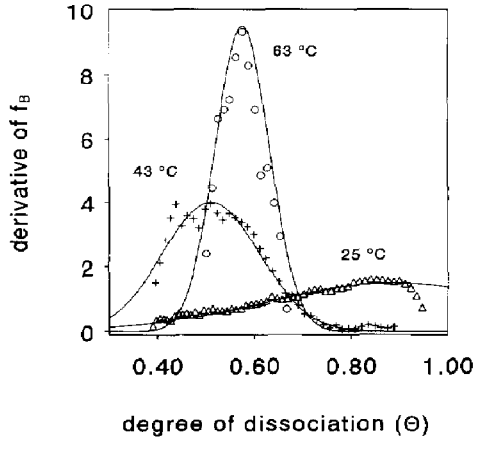

Fig. 2. First derivative of f_B with respect to θ. The cases shown are of 25 and 43°C for Cs = 0.5 mM and of 63°C for Cs = 5 mM. Lines are Gaussian functions, drawn as an aid to the eye. The peak corresponds to θ_{m1}, the midpoint of the first transition.

Table 1
Fitting the composition curves of the first transition

T (°C)	C_1	C_2	$\theta_m = C_2/C_1$	θ_m, from 1st derivative
25 [a]	7.1	6.4	0.9	0.9
43 [a]	19.7	10.3	0.52	0.53
63 [a,b]	31.1	13.5	0.43	0.43
63 [c]	40.6	23.4	0.58	0.58

[a] Cs = 0.5 mM.
[b] These are the constants C_1 and C_2 for the first transition; the second transition with constants C_3 and C_4 is also observed in this case, c.f. Table 2.
[c] Cs = 5 mM.

cases, than did the original branch. Further support of the rescaling method is given in Fig. 5, which is discussed below.

In Fig. 2 the derivatives of the composition curves at 25 and 43°C and Cs = 0.5 mM and of 63°C and Cs = 5 mM are given, which determine the empirical midpoints of transition, θ_m. In all cases the maximum is reached during the titration. Note that the midpoint of transition at 63°C is shifted to a higher value of θ due to the addition of salt. In Table 1 the results of the fits are given, together with both values of θ_m: calculated with Eqn. (7) and obtained from Fig. 2. These results demonstrate that the **A** → **B** transition can be analyzed by fitting the composition curve of f_B to the appropriate expressions of our model. In Fig. 3 the dependence of the constants C_1 and C_2 on the temperature and the salt concentration is given.

The analysis of the **A** → **B** → **C** transition is restricted to one case. The composition curve of f_C at 63°C, which is the result of an iteration process [15], was fitted with a least squares method to Eqn. (6b). Due to the fact that in the iteration the empirical dependence of ln K_i on θ was used, the accuracy of the fit is artificially high. Both the obtained constants and

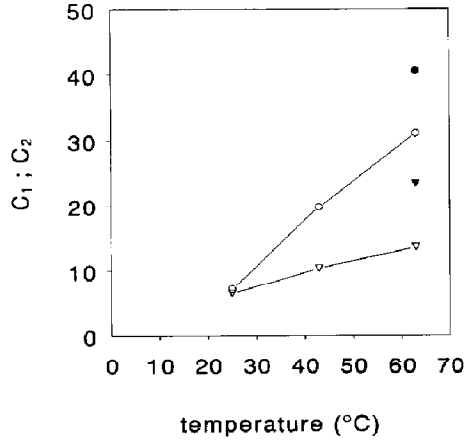

Fig. 3. The dependence of the constants C_1 and C_2 of the **A** → **B** transition on the temperature: ○, C_1, Cs = 0.5 mM; ●, C_1, Cs = 5 mM; ▽, C_2, Cs = 0.5 mM; ▼, C_2, Cs = 5 mM.

Table 2
Fitting the composition curve of the second transition

T (°C)	Cs (mM)	C_3	C_4	$C_4/C_3=\theta_m$
63	0.5	17.3	12.7	0.7

the midpoints of the two transitions demonstrate the consistency of the previous and present methods. The results for the second transition at 63°C are shown in Table 2.

4. Discussion

Dependence of C_1 *and* C_2 *on temperature and salt concentration.*—From the definitions, one has $C_1 = -\delta(\Delta G^0/RT)/\delta\theta$, $C_2 = \{(\Delta G^0)_{\theta=0}\}/RT$, and $\Delta G^0 = G^0_B - G^0_A$. From Table 1 and Fig. 3 it is seen that the stability of uncharged **A** with respect to uncharged **B** increases with increasing temperature. Addition of salt has a similar effect: it stabilizes uncharged **A** with respect to uncharged **B**. Charging xanthan destabilizes *A* with respect to **B** as C_1 is positive. The large temperature dependence of C_1 makes the **A** → **B** transition possible on increasing the temperature at finite charge, i.e., for $\theta > 0.3$; though $(\Delta G^0/RT)_{\theta=0}$ increases with temperature (in favour of a **B** → **A** transition), the even faster increase of $-\delta(\Delta G^0/RT)/\delta\theta$ allows the well known **A** → **B** transition. On the addition of salt at a constant temperature, the **A** → **B** transition shifts to higher charge, i.e., θ_m increases. This is due to two effects: salt stabilizes **A** with respect to **B** even at $\theta=0$ and the screening of the intramolecular electrostatic repulsion increases. It is important to note that C_1 increases on addition of salt: the effect of salt is not restricted to screening electrostatic interaction, it stabilizes the **A** state, reminiscent of a salting-in effect.

Determination of standard free enthalpy.—In the **A** → **B** and **A** → **B** → **C** models, ΔG^0 of the transitions is a function of θ. The value of ΔG^0 of the transition can be calculated at any degree of dissociation θ, with the use of the following relations:

$$\Delta G^0_I(\theta) = -(C_1\cdot\theta - C_2)\cdot RT \qquad \Delta G^0_{II}(\theta) = -(C_3\cdot\theta - C_4)\cdot RT \tag{8}$$

In fact, for each transition a linear relation holds, c.f. Eqs. (2) and (5b). In these linear relations, C_1 and C_3, represent the increment of ΔG^0 upon adding charge to the system. C_2 and C_4 correspond to ΔG^0 of the transitions at zero charge, i.e., taking the uncharged system at $\theta=0$, from state **A** to state **B**, or from state **B** to state **C**. In particular, the values of ΔG^0 at $\theta=0$ and $\theta=1$ are of interest. The former determines the equilibrium constant for the transition of the uncharged polymer, while the latter determines the transition for the fully charged polymer. In Table 3, the values of $(\Delta G^0_I)_{\theta=0}$, $(\Delta G^0_I)_{\theta=1}$, $(\Delta G^0_{II})_{\theta=0}$, and $(\Delta G^0_{II})_{\theta=1}$ are listed.

Temperature dependence of $\Delta G^0(\theta)$.—For the small temperature range under investigation, the following relation for $\Delta G^0(\theta)$ of the first transition is taken to hold with constant $\Delta H^0(\theta)$ and $\Delta S^0(\theta)$.

$$\Delta G^0(\theta) = \Delta H^0(\theta) - T\Delta S^0(\theta) \tag{9}$$

Table 3
The changes of free enthalpy of transition I and II at degrees of dissociation $\theta = 0$ and $\theta = 1$. Cs = 0.5 mM

T (K)	$(\Delta G_I)_{\theta=0}$ (kJ/mol) [a]	$(\Delta G_I)_{\theta=1}$ (kJ/mol) [a]
298	+15.9	−1.7
316	+27.1	−24.7
336	+37.7	−49.2
	$(\Delta G_{II})_{\theta=0}$ (kJ/mol) [a]	$(\Delta G_{II})_{\theta=1}$ (kJ/mol) [a]
336	+35.4	−12.9

[a] Note: the unit "mole" refers to moles of titratable groups.

Table 4
The determination of the thermodynamic quantities ΔH^0 and ΔS^0 of the first transition

Degree of dissociation	ΔH^0 (kJ/mol) [a]	ΔS^0 (J/mol K) [a]	Correlation coefficient
$\theta = 0$	−155	−574	0.9990
$\theta = 1$	+370	+1248	0.9999

[a] The unit "mole" refers to moles of titratable groups.

For brevity, only the values of $(\Delta G_I^0)_{\theta=0}$ and $(\Delta G_I^0)_{\theta=1}$ are listed in Table 3, for the three temperatures investigated. ΔH^0 and ΔS^0 at any θ are obtained by linear regression of the temperature dependence of $\Delta G^0(\theta)$ and plotted in Fig. 4. In Table 4 the values of ΔH^0 and ΔS^0 at $\theta = 0$ and $\theta = 1$ are listed for comparison. From the dependence of the quantities ΔH^0 and ΔS^0 on θ, the following relation is obtained:

$$\Delta G^0 = (525 \cdot \theta - 155) \cdot 10^3 - T \cdot (1822 \cdot \theta - 574) \quad \text{(J/mol)} \tag{10}$$

It should be noted that our data refer to moles of titratable groups in stead of moles of monomer. With the degree of pyruvate substitution equal to 0.5 and one glucuronic acid

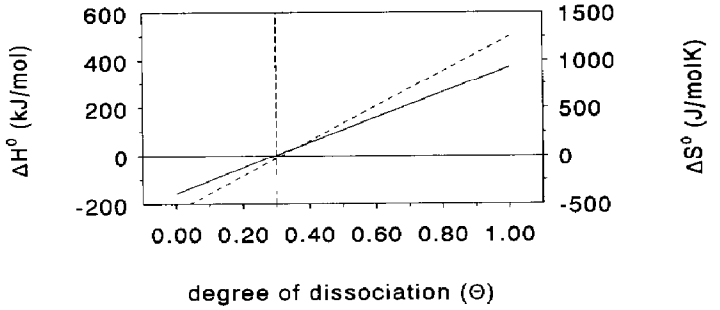

Fig. 4. The dependence of ΔH^0 (drawn line, left axis kJ/mol) and ΔS^0 (dotted line, right axis in J/mol K) on the degree of dissociation θ. Cs = 0.5 mM.

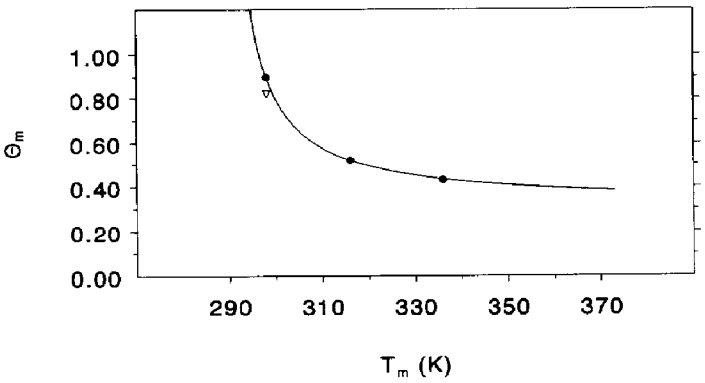

Fig. 5. The correlation diagram of the **A** → **B** transition plotted with Eqn. (11): T_m versus θ_m. Closed symbols (●) are midpoints of the transition obtained from the fits of the composition curves. The open symbol (▽) not fitting the curve is the original, non-rescaled midpoint at 25°C. Cs = 0.5 mM.

residue per monomer [15], 1 mole of titratable groups corresponds with 2/3 mole of monomers. Since by definition $\Delta G^0 = 0$ in the midpoint, one has:

$$\theta_m = \frac{574T_m - 155 \cdot 10^3}{1822T_m - 525 \cdot 10^3} \quad (11)$$

With this relation, the correlation diagram of T_m versus θ_m of Ref [15] can be reconstructed, c.f., Fig 5. Note that the rescaled value of the midpoint for 25°C coincides with the line, while the original value does not. This is a second argument in favour of the rescaling.

The standard enthalpy and entropy.—From the thermodynamic data of Fig. 4 it is seen that the **A** ⇄ **B** equilibrium is entropy determined. At $\theta = 0$, the entropy is higher for the **A** state, whereas, for $\theta > 0.3$ this situation is reversed, and the **B** state has the higher entropy. The enthalpy terms show a similar effect: the uncharged **A** state has the higher enthalpy, whereas, for $\theta > 0.3$, this situation is reversed. For clarity, the transition can only take place for $\theta > 0.3$ no matter what temperature. The dominance of the entropy term is striking: on charging xanthan, the transition from **A** to **B** is therefore *not* only due to a simple destabilization of the **A** state by an increased electrostatic repulsion of charged monomers, but a more complicated mechanism also involving entropic terms is at work.

A possible mechanism for the first transition.—A comparison of the differences of standard enthalpy and entropy for the **A** → **B** transition of xanthan with literature data of conformational transitions in certain proteins, shows that this entropy dominance is not unique. As an example, for the ribonuclease unfolding transition [17], ΔH^0 is of the order +250 kJ/mol and ΔS^0 is of the order +750 J/mol K. Inspection of Table 4 shows that for the first transition of xanthan, these values are of the same order of magnitude for $\theta = 1$. The behaviour of xanthan below $\theta = 0.3$ is, however remarkable: the conformation that is often termed "ordered" is in fact entropy stabilized.

For the first transition of xanthan, single order kinetics was found [9] and since several authors suggested the possibility of the side chain to fold around the backbone [13,18], the **A** → **B** transition might be caused by unfolding of the side chain from the backbone. Due to a gain of conformational freedom around the glycosidic bonds of the side chain upon unfolding, this process is expected to yield a positive contribution to ΔS^0. At $\theta = 0$ however,

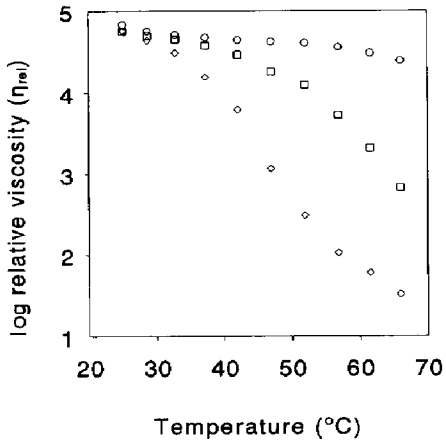

Fig. 6. The logarithm of the relative viscosity against the temperature: ○, $\theta' = 0$ ($0.20 < \theta < 0.27$); □, $\theta' = 0.45$ ($0.48 < \theta < 0.51$); ◇, $\theta' = 0.92$ ($\theta = 0.92$). The degree of dissociation θ, is slightly temperature dependent (values in brackets), hence the temperature independent degree of neutralization, θ', is used. Cs < 0.1 mM, Cp = 3 mM.

unfolding the side chains of the uncharged, hydrophobic polymer increases the hydrophobic surface, at the expense of solvation entropy, which seems to yield a dominant negative contribution. Upon charging the side chains, the hydrophobicity of the polymer disappears, eliminating this negative contribution. This net balance leads to the possibility to destabilize the **A** conformation by increasing the temperature for $\theta > 0.3$.

The apparent decrease of stiffness on charging the polymer, which we observed from viscosimetry [15] supports the abovementioned unfolding process. In Fig. 6 the relative viscosity is shown as a function of temperature for a shear rate of 20 s^{-1} for three degrees of dissociation. It is clearly seen that the decrease of the viscosity with increasing temperature is very small at $\theta' = 0$ in comparison to the effects for $\theta' = 0.45$ and $\theta' = 0.92$.

In the literature, the observations of the invariance of the molecular weight, first order kinetics, and the enhanced mobility of the side chains are also in support of the unfolding mechanism. A typical length scale of interaction of ca. 10 Å was deduced from the screening effect upon the addition of salt [15], again in support of this mechanism.

5. Conclusions

The charge and temperature dependence of the conformational transitions of xanthan were analyzed using an empirical linear dependence of ΔG^0 on the degree of dissociation θ. For the first conformational transition the quantities $\Delta H^0(\theta)$ and $\Delta S^0(\theta)$ were determined. The first transition of xanthan is found to be entropy determined. The uncharged polymer ($\theta = 0$) tends to persist in the **A** state because it is the entropy stabilized state: increasing the temperature only increases this effect. Possibly, hydrophobic interaction causing the folding of the side chains around the backbone generates such entropy effects. For $\theta > 0.3$, **B** becomes the entropy stabilized state and the transition takes place upon heating. From the quantities $\Delta H^0(\theta)$ and $\Delta S^0(\theta)$ a relation is obtained which describes the correlation diagram of T_m versus θ_m at Cs = 0.5 mM. The addition of salt causes an unex-

pected increase of the charge dependent parameter C_1, which shows that the effect of added salt does not only increase the electrostatic screening, but also stabilizes **A** with respect to **B** at $\theta = 0$. If **A** corresponds to a side chain folded structure, then the presence of salt also influences the stability of this structure, which might be a salting-in effect.

Acknowledgements

Mr. J.A. de Kooker and Mr. W. Jesse are kindly thanked for performing the rotational viscosity measurements. This work was supported by The Netherlands Foundation for Chemical Research (SON) with financial aid from The Netherlands Foundation for the Advancement of Pure Research (NWO).

References

[1] A. Jeanes, J.E. Pittsley, and F.R. Senti, *J. Appl. Polym. Sci.*, 5 (1961) 519–526.
[2] F.R. Dintzis, G.E. Babcock, and R. Tobin, *Carbohydr. Res.*, 13 (1970) 257–267.
[3] G. Holzwarth, *Carbohydr. Res.*, 66 (1978) 173–186.
[4] R.K. Prud'homme, G. Froiman, and D.A. Hoagland, *Carbohydr. Res.*, 106 (1982) 225–233.
[5] P.E. Jansson, L. Kenne, and B. Lindberg, *Carbohydr. Res.*, 45 (1975) 275–282.
[6] L.D. Melton, L. Mindt, D.A. Rees, and G.R. Sandersen, *Carbohydr. Res.*, 46 (1976) 245–257.
[7] K. Okuyama, S. Arnott, R. Moorhouse, M.D. Wilkinshaw, E.D.T Atkins, and Ch. Wolf-Ullish, *ACS Symp. Ser.*, 141 (1980) 411–427.
[8] T. Sato, T. Norisuye, and H. Fujita, *Polym. J.*, 16 (1984) 341–350.
[9] I.T. Norton, D.M. Goodall, S.A. Frangou, E.R. Morris, and D.A. Rees, *J. Mol. Biol.*, 175 (1984) 371–394.
[10] G. Holzwarth, *Biochemistry*, 15 (1976) 4333–4339.
[11] E.R. Morris, D.A. Rees, G. Young, M.D. Wilkinshaw, and A. Darke, *J. Mol. Biol.*, 110 (1977) 1–16.
[12] (a) M. Nakasuga and T. Norisuye, *Polym. J.*, 20 (1988) 939–944; (b) W. Liu, T. Sato, T. Norisuye, and H. Fujita, *Carbohydr. Res.*, 160 (1987) 267–281.
[13] E.R. Morris, *ACS Symp. Ser.*, 45 (1977) 81–89.
[14] A. Gamini, J. de Bleijser, and J.C. Leyte, *Carbohydr. Res.*, 220 (1991) 33–47.
[15] L. Bezemer, J.B. Ubbink, J.A. de Kooker, M.E. Kuil, and J.C. Leyte, *Macromolecules*, 26 (1993) 6436–6446.
[16] S. Paoletti, A. Cesàro, and F. Delben, *Carbohydr. Res.*, 123 (1983) 173–178.
[17] C.R. Cantor and P.R. Schimmel, *The Behavior of Biological Macromolecules*, in *Biophysical Chemistry*, Part 3, Freeman, San Francisco, 1980, Chapter 21.
[18] R. Moorhouse, M.D. Walkinshaw, and S. Arnott, *ACS Symp. Ser.*, 45 (1977) 90–101.